Externally triggered renewed bubble nucleation in basaltic magma: The 12 October 2008 eruption at Halema‘uma‘u Overlook vent, Kīlauea, Hawai‘i, USA

Rebecca J. Carey,[1] Michael Manga,[2] Wim Degruyter,[2] Donald Swanson,[3] Bruce Houghton,[4] Tim Orr,[3] and Matthew Patrick[3]

Received 1 June 2012; revised 11 September 2012; accepted 11 September 2012; published 8 November 2012.

[1] From October 2008 until present, dozens of small impulsive explosive eruptions occurred from the Overlook vent on the southeast side of Halema‘uma‘u Crater, at Kīlauea volcano, USA. These eruptions were triggered by rockfalls from the walls of the volcanic vent and conduit onto the top of the lava column. Here we use microtextural observations and data from clasts erupted during the well-characterized 12 October 2008 explosive eruption at Halema‘uma‘u to extend existing models of eruption triggering. We present a potential mechanism for this eruption by combining microtextural observations with existing geophysical and visual data sets. We measure the size and number density of bubbles preserved in juvenile ejecta using 2D images and X-ray microtomography. Our data suggest that accumulations of large bubbles with diameters of >50 μm to at least millimeters existed at shallow levels within the conduit prior to the 12 October 2008 explosion. Furthermore, a high number density of small bubbles <50 μm is measured in the clasts, implying very rapid nucleation of bubbles. Visual observations, combined with preexisting geophysical data, suggest that the impact of rockfalls onto the magma free surface induces pressure changes over short timescales that (1) nucleated new additional bubbles in the shallow conduit leading to high number densities of small bubbles and (2) expanded the preexisting bubbles driving upward acceleration. The trigger of eruption and bubble nucleation is thus external to the degassing system.

Citation: Carey, R. J., M. Manga, W. Degruyter, D. Swanson, B. Houghton, T. Orr, and M. Patrick (2012), Externally triggered renewed bubble nucleation in basaltic magma: The 12 October 2008 eruption at Halema‘uma‘u Overlook vent, Kīlauea, Hawai‘i, USA, *J. Geophys. Res.*, *117*, B11202, doi:10.1029/2012JB009496.

1. Introduction

[2] The diversity in style and intensity of basaltic eruptions are driven by the competing processes of vesiculation (degassing) and the escape of the gas from the ascending magma (outgassing) [e.g., *Mangan et al.*, 1993; *Mangan and Cashman*, 1996; *Parfitt*, 2004; *Edmonds and Gerlach*, 2007; *Edmonds*, 2008; *Houghton and Gonnermann*, 2008]. In such systems, the timing and kinetics of bubble nucleation and volatile exsolution during decompression modulate the degree to which exsolved volatiles remain mechanically coupled to the magma: rapid late degassing and relatively slow outgassing promote energetic and explosive eruption [*Namiki and Manga*, 2008].

[3] Degassing at Kīlauea’s summit is a complex process as the low viscosity of basaltic magma permits melt-vapor separation and two-phase flow that begins with CO_2 degassing at depth, and concludes with predominantly H_2O and SO_2 exsolution from the melt at shallow levels (~100–150 m) [*Gerlach and Graeber*, 1985]. The diversity of eruption styles observed at Kīlauea illustrates the consequences of different combinations of vesiculation, bubble coalescence, and outgassing processes. At high degrees of vapor segregation, coalescence of bubbles increases bubble size and rates of buoyant ascent through the magma. At the Earth’s surface this is manifested as continuous gas emission, gas pistoning, and lava spattering eruption styles [e.g., *Edmonds and Gerlach*, 2007; *Houghton and Gonnermann*, 2008; *Patrick et al.*, 2011b]. High magma ascent rates and lower degrees of vapor segregation lead to reduced timescales for bubble nucleation and growth, generating supersaturation of volatiles, bubble overpressure and rapid late stage acceleration of the magma [e.g., *Proussevitch and Sahagian*, 1996, 1998]. Fountaining episodes of Pu‘u ‘Ō‘ō [*Heliker et al.*, 2003], Mauna Ulu [*Swanson et al.*, 1979], and Kīlauea Iki [*Stovall et al.*, 2011, 2012] are representative

[1]ARC Centre of Excellence in Ore Deposits and School of Earth Science, University of Tasmania, Sandy Bay, Tasmania, Australia.
[2]Department of Earth and Planetary Science, University of California, Berkeley, California, USA.
[3]Hawaiian Volcano Observatory, U.S. Geological Survey, Hawai‘i Volcanoes National Park, Hawai‘i, USA.
[4]Geology and Geophysics Department, University of Hawai‘i at Manoa, Honolulu, Hawai‘i, USA.

Corresponding author: R. J. Carey, ARC Centre of Excellence in Ore Deposits, University of Tasmania, Sandy Bay, Tas 7005, Australia. (rebecca.carey@utas.edu.au)

0148-0227/12/2012JB009496

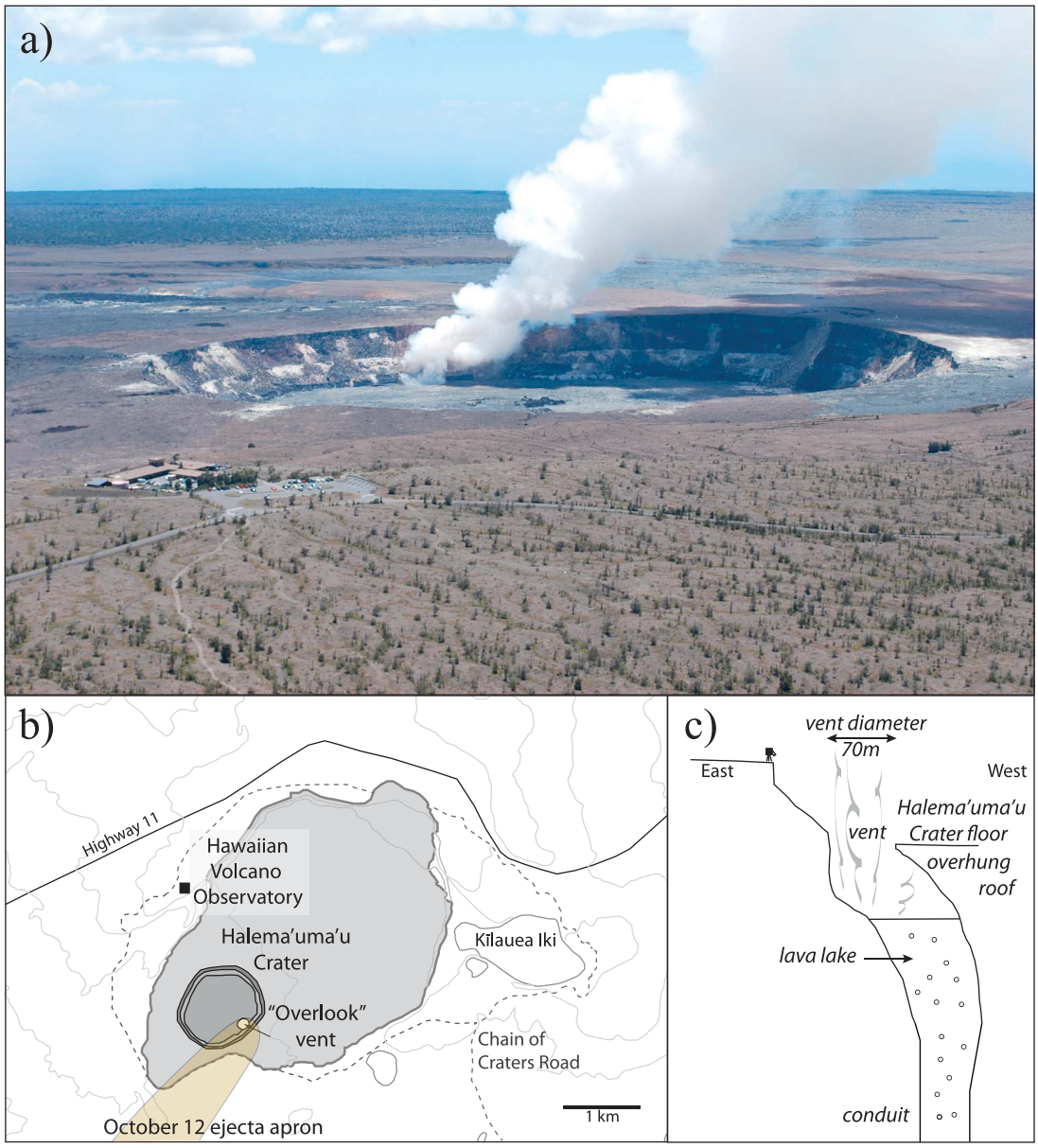

Figure 1. (a) Photo of Halema‘uma‘u crater and the site of the active vent after the 12 October 2008 explosion. The Hawaiian Volcano Observatory can be seen in the foreground. Photo taken by Tim Orr, USGS. (b) Map of Kīlauea caldera outlining the geometry of the summit, the site of the summit eruption and the dispersal area of the 12 October explosion. (c) Cross section cartoon of the vent geometry at the time of the eruption. Note that the roof of the shallow conduit is overhung. At the time of the 12 October explosion, the vent diameter was ~73 m. Observations throughout 2008 to the present day have shown that the magma free surface may rise and fall, associated with gas pistoning, while at other times magma input into the shallow cavity has risen the magma free surface to within 65 m of the floor of Halema‘uma‘u.

of such systems. Our goal here is to assess the dynamics of vesiculation during the 12 October 2008 event using the only physical record of the ascent, degassing and fragmentation of the magma—the juvenile ejecta.

1.1. Ongoing Halema‘uma‘u Eruption

[4] Kīlauea’s ongoing (as of May 2012) summit activity began on 19 March 2008, with the opening of a new eruptive vent, which we call the “Overlook” vent, on the southeast side of Halema‘uma‘u Crater [*Wilson et al.*, 2008; *Swanson et al.*, 2009; *Houghton et al.*, 2011] (Figures 1a and 1b). Throughout 2008, the vent and shallow conduit were steeply inclined and the roof of the vent was overhung (Figure 1c). Vent wall collapses have been common since the onset of the eruption, comprising several hundred events, each of which produced a dusty ash plume [*Orr et al.*, 2012]. The rockfalls were accompanied by high-frequency (HF) seismicity that transitioned into long-period (LP) and very-long-period (VLP) seismicity. The 7 largest triggered weak explosive eruptions that deposited ash- to bomb-sized juvenile magma

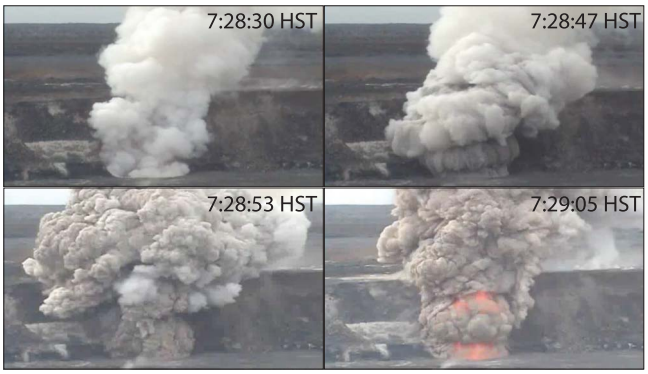

Figure 2. Four images showing the different stages of the eruption on 12 October 2008. (top left) The steam plume present before onset of (top right) the dark ash- and lapill-laden plume. (bottom left) Vigorous degassing pulses dominate the next 30 s, the onset of which is shown, and (bottom right) later become more energetic and incandescence representing high volumes of hot tephra is observed in the dark plume. The eruption lasted for ~80 s and dispersed pyroclasts onto the floor of Halema'uma'u crater and Kīlauea summit.

and lithic fragments up to several hundred meters from the vent [*Orr et al.*, 2008; *Orr et al.*, 2012].

1.2. The 12 October 2008 eruption

[5] Here we focus on the well-constrained eruption of Halema'uma'u on 12 October 2008 [*Patrick et al.*, 2011a]. A small explosive eruption from the Overlook vent occurred at 7:28 A.M. (all times reported in Hawaii standard time) on 12 October (Figure 2). This event ejected juvenile and lithic lapilli and ash over a dispersal area extending more than 700 m from the vent (Figure 1b). *Patrick et al.* [2011a] combined precisely timed visual observations of the eruption with seismicity and infrasound. They showed that the first appearance of the eruption plume at the vent rim occurred at 07:28:42 A.M., just two seconds after the start of an infrasound signal and 5–6 s after the peak of a high frequency seismic burst. During the period of peak infrasound amplitudes (roughly 07:28:42 to 07:28:56 A.M.), pulsing ash emission was seen at the vent. The impact of coarse ejecta on the crater rim was observed in the video beginning at 07:28:57 A.M. Pulsing incandescence began around 07:29:02 A.M., during concurrent ash emission, and continued for about the next 60 s. *Patrick et al.* [2011a] found that the main explosive phase of the eruption overlaps in time with the peak infrasound and VLP amplitudes, suggesting that the VLP seismicity is not due to a rising gas slug, but rather outgassing at the top of the column.

[6] The 12 October eruption was a relatively small event in the broader spectrum of explosive volcanism. Seismically, though, it was the largest explosive eruption of Halema'uma'u during 2008 [*Orr et al.*, 2008; *Wooten et al.*, 2008]. The mass of material erupted during the 12 October eruption, 5×10^4 kg, was estimated based upon the deposit geometry, isomass data, and field measurements of bulk density (Houghton *et al.*, in prep). Conversion of eruptive mass to a dense rock volume was conducted assuming a density of 1000 kg m^{-3} and calculated as 50 m^3. Using a duration of the eruption of 80 s the time-averaged mass and volumetric discharge rates are calculated as 10^3 kg s^{-1} and <1 m^3 s^{-1}. These values are minima but still relatively low on scales of basaltic eruptive intensity [*Houghton and Gonnermann*, 2008].

2. Microtextural Characterization of Eruption Products

[7] We used two complementary approaches to characterize the vesicles in juvenile lapilli. First, we used SEM images at variable magnifications to identify all three phases within the samples: glass, vesicles and crystals (Figure 3). A fourth phase, foreign lithics introduced by the triggering rockfall [*Wooten et al.*, 2008; *Orr et al.*, 2012], is not considered. These measurements allow us to quantify the size distribution and number density of vesicles and we follow the methodology described in *Adams et al.* [2006]. Second, we imaged the three-dimensional texture of clasts using high-resolution X-Ray microtomography (μXRT), using the 8.3.2 beamline at the Advanced Light Source at the Lawrence Berkeley National Laboratories. The three-dimensional (3D) renderings allow us to capture the 3D microstructure of the clast and evaluate the degree of interconnectedness of bubbles. μXRT reconstructions were used only to identify two phases: glass and bubbles (Figure 4).

2.1. Measurements

[8] One-hundred clasts in the 8–16 mm size range were collected from the 12 October ejecta apron and then density was measured following the methods described in *Houghton and Wilson* [1989]. Four pyroclasts that span the modal range of the density spectrum were selected for microtextural analysis. All clast densities are relatively low (310–1100 kg m^{-3}, 89–62 vol.%), 67% of the clasts have density values between 500 and 800 kg m^{-3} (73–83 vol.%). Four clasts were chosen from this modal range (Figure 3).

[9] In thin section, the analyzed pyroclasts show porphyritic textures. The glasses are generally brown in color yet have zones that are alternatively lighter and darker in color. The groundmass crystals are typically sparse (<5 area %), and dominated by clinopyroxene microlites (~20 μm). Lithic inclusions derived from conduit and vent walls are common (1–5 area %) and are composed of both fresh and hydrothermally altered lava.

[10] All clasts, except H08–52, contain numerous vesicles with radii <50 μm that are predominantly round. These small bubbles are often distributed heterogeneously within a clast, but can concentrate around larger bubbles (Figure 3: H08–50). There appears to be no spatial relationship between vesicle and microlite abundances in the groundmass. Intermediate-sized bubbles are more complex with multilobate and cuspate bubble shapes, which is likely a consequence of bubble coalescence. In thin section, H08–51 contains darker glass, fewer and larger bubbles that are commonly stretched, and microlites, microphenocrysts and phenocrysts are more abundant. Lighter-colored areas within this clast are characterized by a heterogeneous distribution of predominantly small (5–50 μm) round bubbles, which are concentrated around larger more complex bubbles. The H08–58 clast has an intermediate density and the most complex vesicle texture of all clasts measured. Intermediate and large bubbles have very complex, convoluted shapes, often with pinched ends, whereas the smallest bubbles are rounded. Intermediate to large bubbles in H08–50 are also complex in

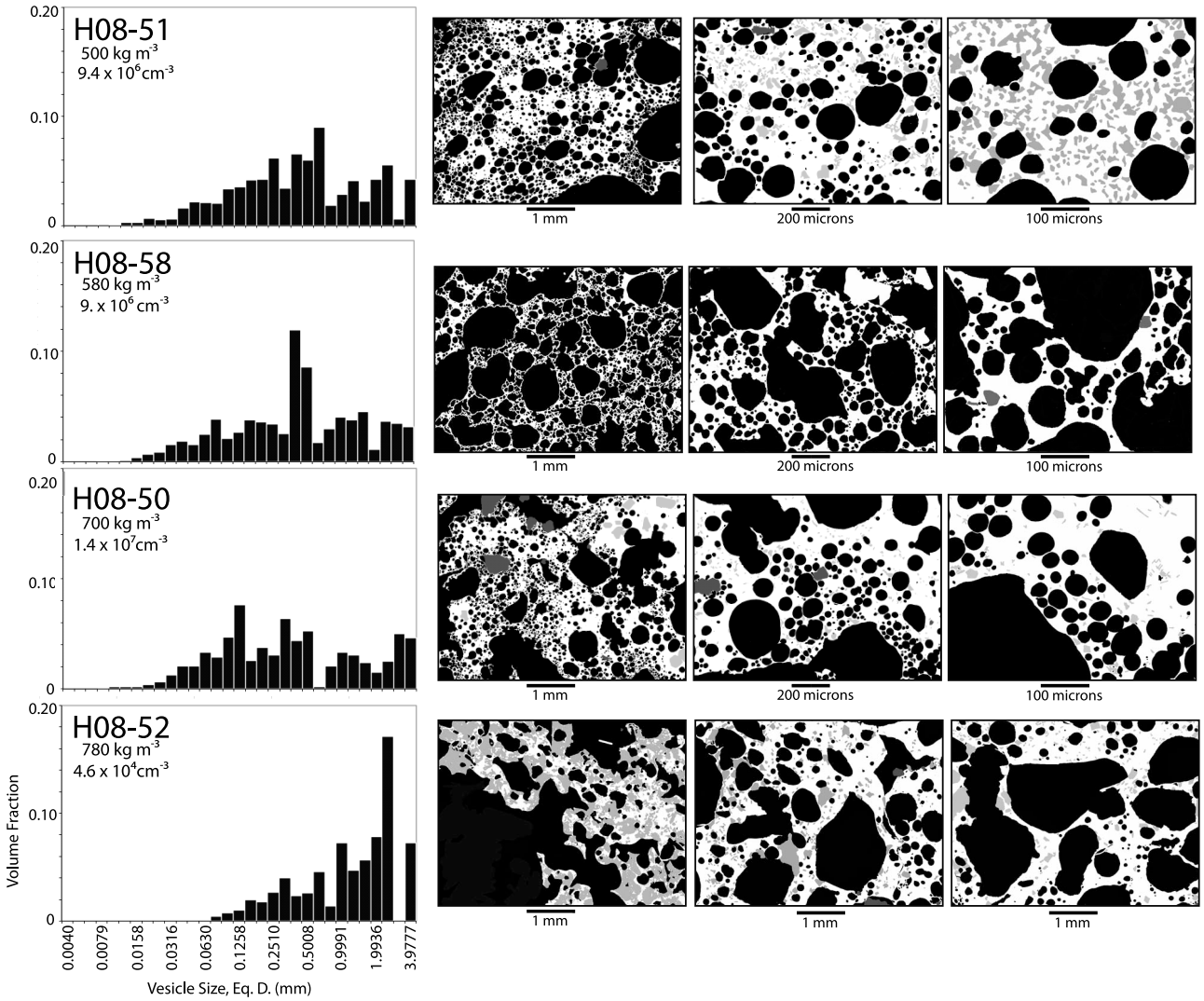

Figure 3. Scanning electron microscope (SEM) images of pyroclast microtextures and 2D vesicle volume distributions for four clasts from the 12 October 2008 explosive eruption. Sample name, juvenile clast densities and vesicle number densities are shown in the upper left corner of the vesicle volume distribution plots. In SEM images white is volcanic glass, light gray are phenocrysts and microlites, dark gray are wall rock xenoliths and black is void space (bubbles). Clast microtextures are variable in bubble size and distribution, however all clasts except H08–52 show 3 orders of magnitude variation in bubble size. Small bubbles <100 μm are typically round, while intermediate (100–1000 μm) and large bubbles (>1 mm) can be both round or complexly shaped.

shape but this is predominantly due to coalescence. The highest density clast of this study, H08–52, also has the most mature bubble texture. The pyroclast shows a variation of glass color from brown to black with the conspicuous absence of golden brown glass. It is coarsely vesicular with many mm-sized bubbles. Bubble shapes are extremely variable, and larger bubbles show the most complex lobate shapes of any clast.

[11] The vesicle volume distribution (VVD) can be separated into two types. The first type has low vesicle number densities (10^4 cm^{-3}) skewed to larger vesicle size (H08–52), representing textural maturity. The second type has much higher vesicle number densities (10^6–10^7 cm^{-3}) and a wide range of vesicle sizes, from 7 μm to 5 mm (H08–51, H08–50, H08–58). The high bubble number density is thus a result of the abundant small bubbles <50 μm, yet they only make up less than 1 vol.% of the clast. This equates to 91–94% of the bubbles residing in this size fraction.

3. Discussion

[12] First we need to establish if the textures preserve the state of the magma near the time of eruption. This is justified by considering two microtextural observations: (1) there is no spatial zoning of larger bubbles within the clast, suggesting that the interior of the clast did not have an extended time above the glass transition to allow bubbles to continue to vesiculate and coalesce, (2) complexly shaped intermediate

and large bubbles are present suggesting that the time for shape relaxation was limited (Figures 3 and 4).

[13] We can calculate the characteristic timescale for bubble relaxation driven by surface tension [e.g., *Toramaru*, 1989; *Rust et al.*, 2003] to evaluate the minimum time (τ_t) between formation of such complex bubble shapes and the quenching time:

$$\tau_r = \frac{r\eta}{\sigma} \quad (1)$$

where r is the bubble radius (m), σ surface tension (0.3 N/m) [*Walker and Mullins*, 1981], η viscosity (100 Pa s) [*Shaw et al.*, 1968]. The calculated characteristic timescales for bubble relaxation with radii between 100 μm and 1 mm are 0.03 to 0.3 s, given a typical Kīlauea melt viscosity (100 Pa s). If we increase the viscosity by an order of magnitude (1000 Pa s) to account for crystallinity, and a vesicular foam with bubble-bubble interactions [*Llewellin and Manga*, 2005], the calculated relaxation timescale would extend to 0.3 to 3 s. Therefore the quenching time after bubble coalescence was likely less than 3 s for these large mm-size bubbles.

[14] We can also compare the time for bubbles to coalesce with the time over which their deformed shapes relax. Bubbles with complex shapes are not stable within a low-viscosity magma foam [*Proussevitch et al.*, 1993a]. At low pressure, differences in pressure between bubbles of contrasting size will expel liquid from films and plateau borders leading to film thinning, rupture and bubble coalescence [*Proussevitch et al.*, 1993a]. In magmatic foams containing bubbles with dimensions <1 cm, surface tension rather than gravitational forces will dominate as the driving force to make bubbles spherical despite the interaction of bubbles and flattening of bubble walls [*Proussevitch et al.*, 1993a). For smaller bubbles, (r < 1 mm), melt films between bubbles are less stable, whereas for larger bubbles, plateau borders are the first to rupture. The maximum timescale of stability (τ) of melt films (τ_f) and plateau borders (τ_p) can be calculated by [*Proussevitch et al.*, 1993a]:

$$\tau_f = \frac{3\eta r^3}{4\sigma}\left(\frac{1}{\delta_{cr}^2} - \frac{1}{\delta_f^2}\right), \quad (2)$$

$$\tau_p = \frac{306\eta r}{\sigma}\ln\left(\frac{\delta_p}{\delta_{cr}}\right), \quad (3)$$

where δ_{cr} is the critical thickness of films or plateau borders, δ_f is the initial thickness of films between bubbles, and δ_p is the initial thickness of plateau borders. Based on SEM and μXRT observations of thin melt films between bubbles of similar size (Figures 3 and 4), we take the critical film thickness (δ_{cr}) to be 0.1 μm, and the characteristic melt film and plateau thickness (δ_f, δ_p) as 10 to 100 μm. The stability timescales for plateau thinning and rupture will be less than that of films for bubbles with radii >1 mm [*Proussevitch et al.*, 1993a]. Complexly

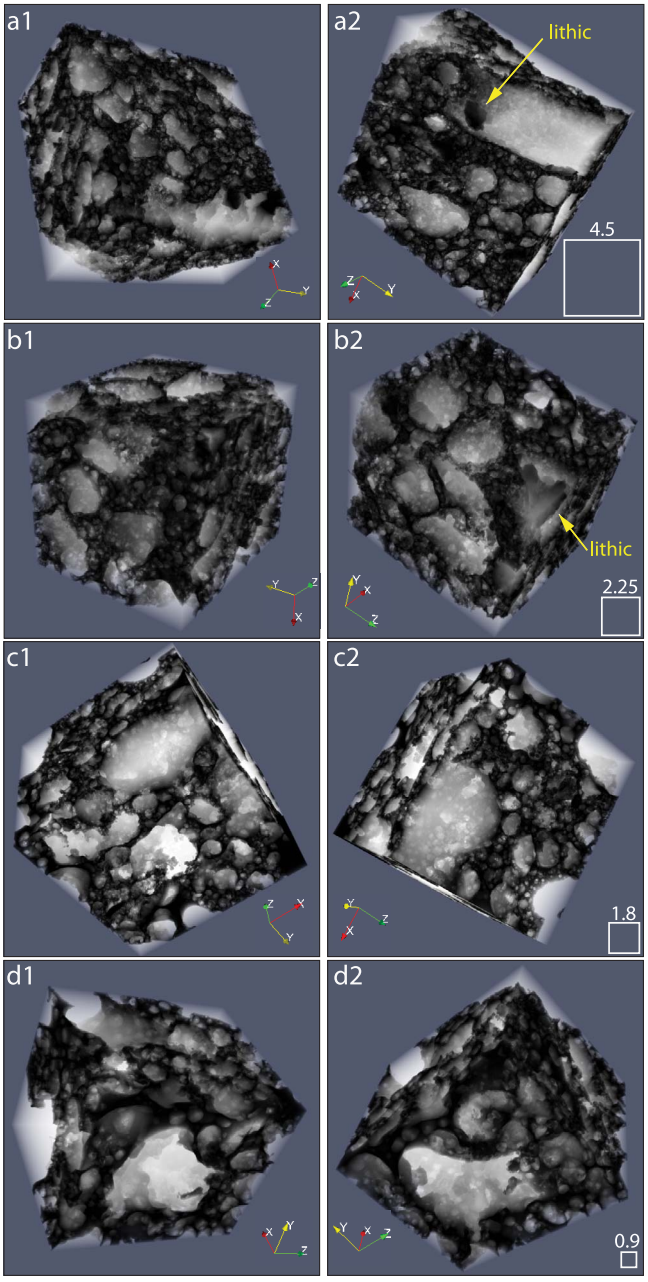

Figure 4. Synchrotron X-Ray microtomography images of a respresentative clast from the modal sample density (most similar to H08–50) are shown here at different image resolutions, as shown by the white boxes and side length (mm) on the bottom right hand side of the figure. Black and white coloring of images is related to glass and pore space, respectively. In Figures 4a2 and 4b2 a dense wall rock lithic can be seen within a vesicle. (a–d) Four different resolutions illustrate the large range of bubble sizes present. Two views of each volume are shown. Cube diameters of largest sides for Figures 4a, 4b, 4c, and 4d are 4.54, 2.25, 1.81, 0.9 mm, respectively. X, Y, Z orientation of the imaged volume is shown by colored axes in corners. The size of clast imaged via tomography and scanning electron microscope were identical. At energies of 20 keV, 1440 projections at 200 ms exposure times were taken while rotating the sample. Two lenses were used to capture the range of bubble sizes in the volume, resulting in pixel sizes of 4.4 and 1.77 microns. The images were cropped in order to capture the inside of the volume. Image segmentation was conducted using 3dma-rock [*Lindquist and Venkatarangan*, 1999] as outlined for volcanic particles in *Degruyter et al.* [2010]. Image visualization was conducted with open source software Paraview.

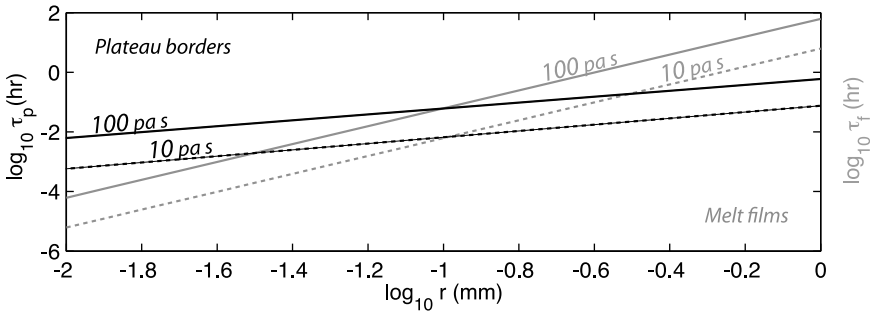

Figure 5. The maximum timescales of stability for melt films (gray) and plateau borders (black) calculated with equations from *Proussevitch et al.* [1993a]. Two different types of calculations using viscosities of either 10 Pa s, or 100 Pa s. The latter takes into account a potential increase in viscosity related to degassing and microlite crystallization.

shaped bubbles of 1 mm size have timescales of plateau stability that are on the order of 10 min given viscosities of 100 Pa s and surface tensions of 0.3 N/m (Figure 5). In contrast, the timescales for relaxation are relatively short (<3 s), for bubble diameters of 100–1000 μm, far less than the timescales for bubble coalescence (Figure 5).

[15] In summary, the absence of bubble zoning and presence of bubbles with complex shapes suggest that the textural signature observed in the clasts is representative of the syn-fragmentation vesicularity of the magma. We can therefore infer that (1) the small bubble population formed syn-eruptively, and (2) a porous bubbly magma existed at shallow levels prior to this eruption. We can thus quantify the dynamics of this eruption based on these textures.

3.1. Small Bubble Population: Model for Bubble Nucleation

[16] The high number density of small bubbles is comparable to that in the most powerful basaltic eruptions (Figure 6) [e.g., *Mangan and Cashman*, 1996; *Mangan et al.*, 1993; *Lautze and Houghton*, 2005, 2007; *Sable et al.*, 2009; *Stovall et al.*, 2011, 2012]. The presence of a high number of small bubbles (<50 μm) implies rapid nucleation as a response to decompression. We now examine if the rockfall could cause this nucleation signature in clasts by (1) estimating if its timescale was fast enough for renewed nucleation, and (2) assessing how the rockfall could generate a decompression large enough to generate the large bubble number density in 12 October 2008 clasts.

[17] The rockfall can nucleate bubbles in either of two ways. The first is by disrupting the crust on the convecting lava to expose melt below the surface to a lower pressure. The second is through the pressure wave generated by the impact itself. The decompression component of this wave will lead to (temporarily) supersaturated conditions. In both cases, new bubbles will nucleate only if the system is decompressed faster than the volatiles can diffuse into the preexisting bubbles [e.g., *Proussevitch et al.*, 1993b]. This depends on the time for diffusion (τ_{diff}), compared with the time scale over which pressure changes, τ_{p}. The ratio of the timescales is a Peclet number, which can be used to assess whether diffusion will occur over the time scale of the pressure variation. The timescale of diffusion is $\tau_{\mathrm{diff}} \sim \mathrm{O}(l^2/D)$, where l is the thickness of melt films surrounding the preexisting bubbles, and D is the diffusivity of water. The notation O() is used to denote order of magnitude values and scalings.

[18] The SEM data indicate a thickness of melt films between bubbles of ~10 μm. The high-frequency seismic event related to the rockfall impact [*Wilson et al.*, 2008; *Patrick et al.*, 2011a] constrain the timescales τ_{p} to about 1 s. Using a diffusivity of 5×10^{-11} m^2 [*Zhang et al.*, 2007] gives Peclet numbers of ~2. For melt supersaturation on this timescale, the Peclet number must be >O(1), consistent with order-or-magnitude estimates for our clasts. A supplementary consideration in this system is that bubble walls cool around fast-growing bubbles [*Sahagian and Proussevitch*, 1996], which would further lengthen the timescale of volatile diffusion into bubbles.

[19] The supersaturation developed during decompression may be able to nucleate bubbles. We assume that the only relevant volatile species is H_2O, at these shallow depths, and adopt the same formulation for the nucleation rate J based on classical nucleation theory used in other studies [e.g., *Mangan and Sisson*, 2000]:

$$J = \frac{2n_o^2 V_m D(\phi\sigma/kT)^{1/2}}{a_o} \exp\left[-\frac{16\pi\sigma^3}{3kT\Delta P^2}\phi\right] = J_o \exp\left[-\frac{16\pi\sigma^3}{3kT\Delta P^2}\varphi\right] \tag{4}$$

where n_{o} is the number density of dissolved water molecules, V_{m} is the volume of the water molecule, k is the Boltzmann constant, T is temperature, a_{o} is the mean distance between water molecules, and ΔP is the supersaturation pressure. ϕ is a factor that accounts for a decrease in surface energy for heterogeneous nucleation, likely to be the case for nucleation that triggers eruptions [*Gardner and Denis*, 2004]. There are no nucleation studies for basaltic liquids that provide ϕ. We thus use the product of $\sigma^3\phi = 7.6 \times 10^{-7}$ N^3/m^3 from *Hurwitz and Navon* [1994], the combination of parameters that controls the ability of bubbles to nucleate. We obtain diffusivity from *Zhang et al.* [2007] for water in basalt.

[20] We assume that nucleation occurs during a sinusoidal decompression wave.

$$P(t) = P_0 \sin\left(2\pi t/\tau_{\mathrm{p}}\right) \tag{5}$$

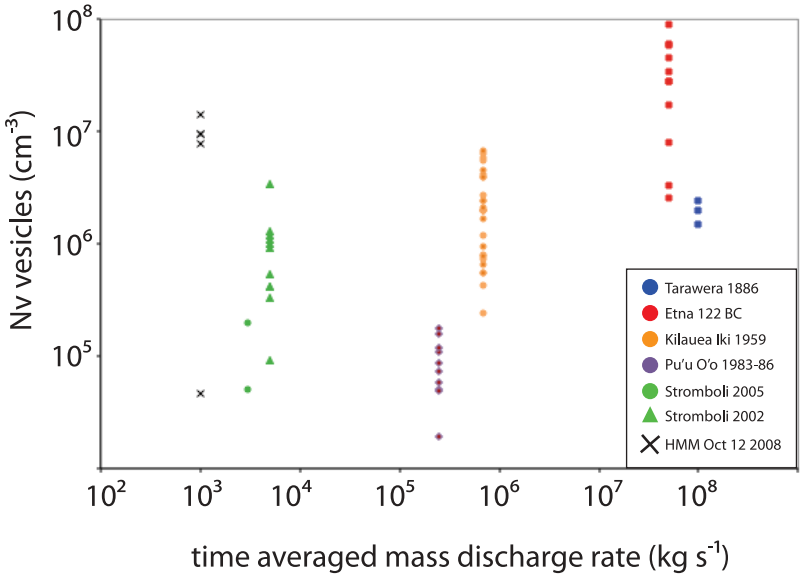

Figure 6. Vesicle number density (N_v) versus time averaged mass discharge rates for basaltic explosive eruptions. The 12 October explosion data plot at high vesicle number densities, yet the time-averaged mass discharge data plot significantly lower than other eruptions with similar vesicle number densities. Data from *Mangan et al.* [1993], *Mangan and Cashman* [1996], *Lautze and Houghton* [2005], *Lautze and Houghton* [2007], *Sable et al.* [2006, 2009], and *Stovall et al.* [2011, 2012].

The total number of bubbles nucleated (neglecting diffusion into preexisting bubbles) is then,

$$N = \int_0^{\pi T} J dt = J_o T \pi \mathrm{erfc} \sqrt{16\pi\sigma^3\phi/3kTP_o^2} \qquad (6)$$

For volatile contents of 0.2 and 2 wt.% water and a timescale of the pressure change of 1 s, calculations suggest that pressure amplitudes must exceed 4 and 3.6 MPa for nucleation of 10^7 cm^{-3} bubbles. To achieve such pressure changes by breaking the crust requires exposing melt at depths >100 m to the atmosphere, but the impact of the rockfall likely cannot penetrate to such large depths. We emphasize the considerable uncertainty in the parameters in equation (4) and note that this nucleation model has not been tested for basalt. All derived numerical values and results are thus best viewed as order-of-magnitude estimates.

[21] Can the impact of the rockfall on the magma free surface generate a few MPa of pressure required for renewed nucleation? The impact pressure can be calculated by assuming momentum and mass are conserved during the collision. Immediately below the impact site, if the impact velocity is small compared to the bulk sound speed, the collision will generate a pressure wave with pressure P given by [*Melosh*, 1989, section 3.2],

$$P = \rho_m c U, \qquad (7)$$

where ρ_m is the magma density, c is the shock velocity which is equal to the bulk sound velocity at low-impact speeds (3.5 km s^{-1} for basalt) [*Sekine et al.*, 2008], and U is the particle velocity, equal to half the impact velocity if the impactor and target are the same material. Using a bulk density of 1000 kg m^{-3} and an impact velocity on the order of 30 ms^{-1} (ballistic speed of the rockfall when it reaches the surface) gives peak (compression) pressures of ~100 MPa. Bubbles will reduce the bulk sound speed; using the theoretical relationship of *Mackenzie* [1950] and a ratio of bulk and shear moduli measured for basalt [*Manghnani and Woollard*, 1965], vesicularities of 30–60% will reduce c by 20–31%. We assume that the pressure is not dampened, which is reasonable at the surface. Our estimate is therefore a maximum. Nucleation of new bubbles must occur in the decompression that accompanies rebound, but owing to dissipation, rebound pressure wave velocities will be smaller. Assuming a modest restitution coefficient of 0.2 [*Dufek et al.*, 2009] a rebound pressure wave will still lead to decompressions of 20 MPa. Despite considerable uncertainties, the order of magnitude of these pressures are large enough to nucleate bubbles or induce cavitation to provide the nuclei for new bubbles.

3.2. Large Bubble Population: Driving the Eruption

[22] The 12 October clast microtextures show a combination of large (mm-size), complexly shaped and round bubbles often in intimate contact with high numbers of small (5–50 μm) round bubbles (Figures 3 and 4). The 12 October juvenile ejecta have vesicularities between 62 and 89 vol.% suggesting that the magma was porous prior to the rockfall. The energy available to drive the eruption is thus likely stored in the potential energy in the preexisting larger bubbles [*Carey et al.*, 2012]. A velocity of basalt fragments ejected from the free surface can be calculated by converting this energy to kinetic energy [e.g., *Namiki and Manga*, 2008],

$$v = \sqrt{\frac{2\gamma\phi P_{ex}}{\rho_m(1-\phi)(\gamma-1)}} \qquad (8)$$

where γ is the isentropic exponent and we neglect other energy sources such as the initial kinetic energy of the magma. We assume that the rockfall generates stresses that are large enough to break the crust. Disruption quickly exposes the underlying magma to a lower pressure. P_{ex} can be estimated as $\rho_m \phi g d$, where d is the depth to which magma is exposed to decompression, and ϕ is the porosity of the magma prior to eruption. For ϕ between 50 and 70%, which is similar to the minimum vesicularity of the tephra erupted, and likely a good preexpansion value, and d = 10–50 m, plausible disruption depths of rockfall, we obtain ejection velocities in the range of 19–75 m s^{-1}. Contemporaneous with the ash-laden plume, this velocity is sufficient to eject juvenile magma to the crater floor.

4. Interpretation

[23] We have used microtextural data from juvenile clasts ejected during the 12 October 2008 eruption to probe the relationship between vesiculation and the role of external influences (in this case, rockfall), on eruption dynamics. We use these data to answer the following questions: Can the impact of rockfalls into the top of an active lava-filled conduit trigger renewed nucleation of bubbles, and does late-stage nucleation play a role in driving the eruption? What insight can be gained from this explosive eruption of Kīlauea, and what does it contribute to our understanding of basaltic volcanism?

4.1. Can Conditions at Halema‘uma‘u Trigger Nucleation?

[24] The visual observations and geophysical data comprehensively show the link between the rockfall and the ejecta [*Orr et al.*, 2012]. Our microtextural analysis of the ejected clasts shows an unusual nucleation signature of high number densities of small round bubbles. We propose that rockfalls generate pressure amplitudes large enough to trigger a renewed phase of nucleation at shallow levels in the conduit.

4.2. What is the Role of the Rockfalls at Halema‘uma‘u?

[25] The new bubbles nucleated by the impact of the rockfall probably do not play a role in the eruption as they are not volumetrically dominant after formation, and their expansion is minimal on the timescale of the eruption. They are primarily “tracers” of the energy delivered by the rockfall to disrupt the crust on timescales short enough to allow preexisting bubbles to drive a small eruption.

[26] *Orr et al.* [2012] show that rockfalls onto the lava lake surface generate a rebound splash, called a Worthington jet. Videos of recent (2011–2012) rockfalls show that pyroclasts are produced during this splash and can be transported out of the vent. However, while the splash mechanism can expel clasts, it cannot produce the decompression required for the volume or timescales of pyroclast production as measured on 12 October 2008.

[27] The 12 October clast data suggest that porous magma with bubbles of diameter 5 μm to at least 5 mm, exist at, or very close to, the free surface prior to the explosion. There is sufficient potential energy in the preexisting bubbles to drive the eruption. We suggest that both the Worthington jet, and the expansion of preexisting bubbles produce pyroclasts, however the eruption was driven by expansion of preexisting bubbles as a consequence of rapid decompression.

4.3. What is the Role of External Triggers at Basaltic Volcanoes?

[28] We proposed a model to explain how renewed nucleation can be produced by rockfall. However, nucleation of new bubbles was not the driving mechanism of the 12 October eruption. Rather, we suggest that the energy available to drive the eruption was stored in the potential energy in preexisting larger bubbles. These bubbles likely exist within the shallow conduit to a few hundred meters. Therefore in any system where magmas are actively vesiculating and preexisting bubbles exist, e.g., tops of magma chambers [e.g., *Vergniolle and Jaupart*, 1990], or beneath the crustal lids in lava lakes and filled conduits [e.g., *Landi et al.*, 2011], rapid exposure of magma to changes of pressure can result in an (at least weak) explosive eruption. *Landi et al.* [2011] outline the shallow feeding system at Stromboli where the upper part of the conduit possibly works as a buried lava lake. Potentially such shallow conduit geometries with conduit bubble accumulation zones [e.g., *Métrich et al.*, 2005; *Lautze and Houghton*, 2007; *Polacci et al.*, 2009; *Pistolesi et al.*, 2011] could favor an external triggering mechanism.

4.4. Classifications for Basaltic Explosive Eruptions

[29] The eruptive activity on 12 October does not fit with typical preconceptions of low-viscosity basaltic eruptions, because it is linked to external shallow controls. Rockfall-driven explosive eruptions punctuate persistent continuous degassing and outgassing of the magma column. They are weak explosive events that lie in an ill-defined region in the spectrum between coupled and decoupled melt-vapor behavior, i.e., between Hawaiian fountaining and Strombolitype explosions. High vesicle number densities could suggest rapid acceleration of the magma and “inefficient” degassing (Figure 6), but this interpretation is not supported by the geometry, dispersal and volume of the deposit produced. However, the diversity of bubble sizes and shapes hosted within small clast volumes suggests variable timescales for vesiculation and vapor segregation.

[30] The 12 October 2008 eruption does not fall into end-members of either inefficient outgassing (i.e., Hawaiian), or efficient outgassing (i.e., Strombolian) of basaltic magmas; intermediate (mm-cm) and large (dm) bubbles segregate from the melt, yet newly nucleated bubbles are coupled on the timescale of the eruption. Based on the 2008 eruption data described here, classifying basaltic eruptions based on either duration, vesicle number density or discharge rate is over simplified; it is helpful to select parameters that incorporate the properties (and degree of coupling) of both the gas and the melt phase, in addition to the trigger of eruption (ascent versus external trigger) in future classification systems.

4.5. Concluding Remarks

[31] This study has outlined how an external influence, a rockfall onto the lava lake, triggered the explosive eruption of 12 October 2008 at Kīlauea. Rockfalls onto the lava lake surface generated decompression pressures sufficient to trigger bubble nucleation. In the erupted clasts, preserved high vesicle number densities are tracers of this pressure change. The renewed phase of bubble nucleation is not, however,

responsible for driving the eruption. The signature of this mechanism within erupted clasts is the presence of bubbles that range in size across 3 orders of magnitude, have both round and complex shapes, and have high bubble number densities ($>10^5$ cm^{-3}).

[32] **Acknowledgments.** This research was supported by NSF grants EAR-1049662 and EAR-0810332 and USGS grant SV-ARRA-0004. The XRT analyses were conducted at the Advanced Light Source at the Lawrence Berkeley National Laboratories in Berkeley, California, USA. We wish to thank Alastair McDowell, and Dula Parkinson for technical assistance.

References

Adams, N. A., B. F. Houghton, and W. Hildreth (2006), Abrupt transitions during sustained explosive eruptions: Examples from the 1912 eruption of Novarupta, Alaska, *Bull. Volcanol.*, *69*, 189–206, doi:10.1007/s00445-006-0067-4.

Carey, R. J., M. Manga, W. Degruyter, H. Gonnermann, D. Swanson, B. F. Houghton, T. Orr, and M. Patrick (2012), Convection in a volcanic conduit recorded by bubbles, *Geology*, in press.

Degruyter, W., O. Bachmann, and A. Burgisser (2010), Controls on magma permeability in the volcanic conduit during the climactic phase of the Kos Plateau Tuff eruption (Aegean Arc), *Bull. Volcanol.*, *72*, 63–74, doi:10.1007/s00445-009-0302-x.

Dufek, J., J. Wexler, and M. Manga (2009), The transport capacity of pyroclastic flows: Experiments and models of substrate-flow interaction, *J. Geophys. Res.*, *114*, B11203, doi:10.1029/2008JB006216.

Edmonds, M. (2008), New geochemical insights into volcanic degassing, *Philos. Trans. A*, *366*, 4559–4579.

Edmonds, M., and T. M. Gerlach (2007), Vapor Segregation and loss in basaltic melts, *Geology*, *35*, 751–754, doi:10.1130/2FG23464A.1.

Gardner, J. E., and H. M. Denis (2004), Heterogeneous bubble nucleation on Fe-Ti oxide crystals in high-silica rhyolitic melts, *Geochim. Cosmochim. Acta*, *68*, 3587–3597, doi:10.1016/j.gca.2004.02.021.

Gerlach, D. C., and E. J. Graeber (1985), Volatile budget of Kīlauea volcano, *Nature*, *313*, 273–277, doi:10.1038/313273a0.

Heliker, C. C., J. Kauahikaua, D. R. Sherrod, M. Lisowski, and P. F. Cervelli (2003), The rise and fall of Pu'u 'O'o cone, 1983–2002, *U.S. Geol. Surv. Prof. Pap.*, *1676*, 29–51.

Houghton, B. F., and H. M. Gonnermann (2008), Basaltic explosive volcanism: Constraints from deposits and models, *Chem. Erde*, *68*, 117–140, doi:10.1016/j.chemer.2008.04.002.

Houghton, B. F., and C. J. N. Wilson (1989), A vesicularity index for pyroclastic deposits, *Bull. Volcanol.*, *51*, 451–462, doi:10.1007/BF01078811.

Houghton, B. F., D. A. Swanson, R. J. Carey, J. Rausch, and A. J. Sutton (2011), Pigeonholing pyroclasts: Insights from the 19 March 2008 explosive eruption of Kīlauea Volcano, *Geology*, *39*, 263–266, doi:10.1130/G31509.1.

Hurwitz, S., and O. Navon (1994), Bubble nucleation in rhyolitic melts: Experiments at high pressure, temperature, and water content, *Earth Planet. Sci. Lett.*, *122*, 267–280, doi:10.1016/0012-821X(94)90001-9.

Landi, P., E. Marchetti, S. La Felice, M. Ripepe, and M. Rosi (2011), Integrated petrochemical and geophysical data reveals thermal distribution of the feeding conduits at Stromboli volcano, Italy, *Geophys. Res. Lett.*, *38*, L08305, doi:10.1029/2010GL046296.

Lautze, N. C., and B. F. Houghton (2005), Physical mingling of magma and complex eruption dynamics in the shallow conduit at Stromboli volcano, Italy, *Geology*, *33*, 425–428, doi:10.1130/G21325.1.

Lautze, N. C., and B. F. Houghton (2007), Linking variable explosion style and magma textures during 2002 at Stromboli volcano, Italy, *Bull. Volcanol.*, *69*, 445–460, doi:10.1007/s00445-006-0086-1.

Lindquist, W. B., and A. Venkatarangan (1999), Investigating 3D geometry of porous media from high resolution images, *Phys. Chem. Earth*, *25*, 593–599, doi:10.1016/S1464-1895(99)00085-x.

Llewellin, E. W., and M. Manga (2005), Bubble suspension rheology and implications for conduit flow, *J. Volcanol. Geotherm. Res.*, *143*, 205–217, doi:10.1016/j.jvolgeores.2004.09.018.

Mackenzie, J. K. (1950), The elastic constants of a solid containing spherical holes, *Proc. Phys. Soc. London, Sec. B*, *63*, 2–11, doi:10.1088/0370-1301/63/1/302.

Mangan, M. T., and K. V. Cashman (1996), The structure of basaltic scoria and reticulate and inferences for vesiculation, foam formation, and fragmentation in lava fountains, *J. Volcanol. Geotherm. Res.*, *73*, 1–18, doi:10.1016/0377-0273(96)00018-2.

Mangan, M. T., and T. W. Sisson (2000), Delayed, disequilibrium degassing in rhyolite magma: Decompression experiments and implications for explosive volcanism, *Earth Planet. Sci. Lett.*, *183*, 441–455, doi:10.1016/S0012-821X(00)00299-5.

Mangan, M. T., K. V. Cashman, and S. Newman (1993), Vesiculation of basaltic magma during eruption, *Geology*, *21*, 157–160, doi:10.1130/0091-7613(1993)021<0157:VOBMDE>2.3.CO;2.

Manghnani, M. H., and G. P. Woollard (1965), Ultrasonic velocities and related elastic properties of Hawaiian basaltic rocks, *Pac. Sci.*, *19*, 291–295.

Melosh, H. J. (1989), *Impact Cratering: A Geologic Process*, Oxford Univ. Press, New York.

Métrich, N., A. Bertagnini, P. Landi, M. Rosi, and O. Belhadj (2005), Triggering mechanism at the origin of paroxysms at Stromboli (Aeolian Archipelago, Italy): The 5 April 2003 eruption, *Geophys. Res. Lett.*, *32*, L10305, doi:10.1029/2004GL022257.

Namiki, A., and M. Manga (2008), Transition between fragmentation and permeable outgassing of low viscosity magmas, *J. Volcanol. Geotherm. Res.*, *169*, 48–60, doi:10.1016/j.jvolgeores.2007.07.020.

Orr, T. R., M. R. Patrick, K. M. Wooten, D. A. Swanson, T. Elias, A. J. Sutton, D. C. Wilson, and M. P. Poland (2008), Explosions, tephra, and lava: A chronology of the 2008 summit eruption of Kilauea Volcano, Hawaii, *Eos Trans. AGU*, *89*(53), Fall Meet. Suppl., Abstract V11B-2018.

Orr, T. R., M. R. Patrick, D. A. Swanson, A. Weston, A. Thelen, and D. C. Wilson (2012), Explosive eruptions triggered by rockfalls at Kīlauea Volcano, Hawai'i, *Geology*, in press.

Parfitt, E. A. (2004), A discussion of the mechanisms of explosive basaltic eruptions, *J. Volcanol. Geotherm. Res.*, *134*, 77–107, doi:10.1016/j.jvolgeores.2004.01.002.

Patrick, M. R., D. Wilson, D. Fee, T. Orr, and D. A. Swanson (2011a), Shallow degassing events as a trigger for very-long-period seismicity at Kīlauea Volcano, Hawai'i, *Bull. Volcanol.*, *73*, 1179–1186, doi:10.1007/s00445-011-0475-y.

Patrick, M. R., T. Orr, D. Wilson, D. Dow, and R. Freeman (2011b), Cycles of spattering, seismic tremor and surface fluctuations within a perched lava channel, Kīlauea Volcano, *Bull. Volcanol.*, *73*, 639–653, doi:10.1007/s00445-010-0431-2.

Pistolesi, M., D. Delle Donne, L. Pioli, M. Rosi, and M. Ripepe (2011), The 15 March 2007 explosive crisis at Stromboli volcano, Italy: Assessing physical parameters through a multidisciplinary approach, *J. Geophys. Res.*, *116*, B12206, doi:10.1029/2011JB008527.

Polacci, M., D. R. Baker, L. Mancini, S. Favretto, and R. J. Hill (2009), Vesiculation in magmas from Stromboli and implications for normal Strombolian activity and paroxysmal explosions in basaltic systems, *J. Geophys. Res.*, *114*, B01206, doi:10.1029/2008JB005672.

Proussevitch, A. A., and D. L. Sahagian (1996), Dynamics of coupled diffusive and decompressive bubble growth prior to volcanic eruption, *J. Geophys. Res.*, *101*, 17,447–17,455, doi:10.1029/96JB01342.

Proussevitch, A. A., and D. L. Sahagian (1998), Dynamics and energetics of bubble growth in magmas: Analytical formulation and numerical modeling, *J. Geophys. Res.*, *103*, 18,223–18,251, doi:10.1029/98JB00906.

Proussevitch, A. A., D. L. Sahagian, and V. Kutolin (1993a), Stability of foams in silicate melts, *J. Volcanol. Geotherm. Res.*, *59*, 161–178, doi:10.1016/0377-0273(93)90084-5.

Proussevitch, A. A., D. L. Sahagian, and A. T. Anderson (1993b), Dynamics of diffusive bubble growth in magmas: Isothermal case, *J. Geophys. Res.*, *98*, 22,283–22,307, doi:10.1029/93JB02027.

Rust, A. C., M. Manga, and K. V. Cashman (2003), Determining flow type, shear rate and shear stress in magmas from bubble shapes and orientations, *J. Volcanol. Geotherm. Res.*, *122*, 111–132, doi:10.1016/S0377-0273(02)00487-0.

Sable, J. E., B. F. Houghton, P. Del Carlo, and M. Coltelli (2006), Changing conditions of magma ascent and fragmentation during the Etna 122 BC basaltic Plinian eruption: Evidence from clast microtextures, *J. Volcanol. Geotherm. Res.*, *158*, 333–354, doi:10.1016/j.jvolgeores.2006.07.006.

Sable, J. E., B. F. Houghton, C. J. N. Wilson, and R. J. Carey (2009), Eruption mechanisms during the climax of the Tarawera 1886 basaltic Plinian eruption inferred from microtextural characteristics of the deposits, in *Studies in Volcanology: The Legacy of George Walker*, *Spec. Publ. IAVCEI*, vol. 2, pp. 129–154, Geol. Soc., London.

Sahagian, D. L., and A. A. Proussevitch (1996), Thermal effects of magma degassing, *J. Volcanol. Geotherm. Res.*, *74*, 19–38, doi:10.1016/S0377-0273(96)00047-9.

Sekine, T., T. Kobayashi, M. Nishio, and E. Takahashi (2008), Shock equation of state of basalt, *Earth Planets Space*, *60*, 999–1003.

Shaw, H. R., T. L. Wright, D. L. Peck, and R. Okamura (1968), The viscosity of basaltic magma; an analysis of field measurements in Makaopuhi lava lake, Hawaii, *Am. J. Sci.*, *266*, 225–264, doi:10.2475/ajs.266.4.225.

Stovall, W. K., B. F. Houghton, H. M. Gonnermann, S. A. Fagents, and D. A. Swanson (2011), Eruption dynamics of Hawaiian-style fountains: The case study of episode 1 of the Kīlauea Iki 1959 eruption, *Bull. Volcanol.*, *73*, 511–529, doi:10.1007/s00445-010-0426-z.

Stovall, W. K., B. F. Houghton, J. E. Hammer, S. A. Fagents, and D. A. Swanson (2012), Vesiculation of high fountaining Hawaiian eruptions: Episodes 15 and 16 of 1959 Kīlauea Iki, *Bull. Volcanol.*, *74*, 441–455, doi:10.1007/s00445-011-0531-7.

Swanson, D. A., D. A. Duffield, D. B. Jackson, and D. W. Peterson (1979), Chronological narrative of the 1969–71 Mauna Ulu eruption of Kīlauea Volcano, Hawai'i, *U.S. Geol. Surv. Prof. Pap.*, *1056*, 55 pp.

Swanson, D. A., K. Wooten, and T. Orr (2009), Buckets of ash track tephra flux from Halema'uma'u crater, Hawaii, *Eos Trans. AGU*, *90*, 427–428, doi:10.1029/2009EO460003.

Toramaru, A. (1989), Vesiculation process and bubble size distributions in ascending magmas with constant velocities, *J. Geophys. Res.*, *94*, 17,523–17,542, doi:10.1029/JB094iB12p17523.

Vergniolle, S., and C. Jaupart (1990), Dynamics of degassing at Kīlauea Volcano, Hawai'i, *J. Geophys. Res.*, *95*, 2793–2809, doi:10.1029/JB095iB03p02793.

Walker, D., and O. Mullins (1981), Surface tension of natural silicate melts from 1200°–1500°C and implications for melt structure, *Contrib. Mineral. Petrol.*, *76*, 455–462, doi:10.1007/BF00371487.

Wilson, D., T. Elias, T. Orr, M. Patrick, A. J. Sutton, and D. Swanson (2008), Small explosion from new vent at Kīlauea's summit, *Eos Trans. AGU*, *89*, 203, doi:10.1029/2008EO220003.

Wooten, K., C. R. Thornber, D. A. Swanson, J. F. Ellis, T. R. Orr, M. R. Patrick, and J. Rausch (2008), Eruption products and collection methods for the 2008 summit eruption of Kilauea Volcano, Hawai'i, *Eos Trans. AGU*, *89*(53), Fall Meet. Suppl., Abstract V11B-2020.

Zhang, Y., Z. Xu, M. Zhu, and H. Wang (2007), Silicate melt properties and volcanic eruptions, *Rev. Geophys.*, *45*, RG4004, doi:10.1029/2006RG000216.